Int. J. Heat Mass Transfer. Vol. 26, No. 11, pp. 1649-1660, 1983
Printed in Great Britain

0017-9310/83 $3.00 + 0.00
Pergamon Press Ltd.

RADIATIVE SCATTER BY FLY ASH IN PULVERIZED-COAL-FIRED FURNACES: APPLICATION OF THE MONTE CARLO METHOD TO ANISOTROPIC SCATTER

R. P. GUPTA, T. F. WALL and J. S. TRUELOVE
Department of Chemical Engineering, University of Newcastle, NSW 2308, Australia

(*Received* 12 *August* 1982 *and in final form* 8 *March* 1983)

Abstract—The absorption, scatter and extinction efficiencies of a fly ash cloud are shown to have a primary dependence on the complex absorption index of the particles with a secondary dependence on temperature and particle size distribution. The Monte Carlo method is then used to predict radiative transfer in a slab and cylindrical furnace enclosures. Approximating anisotropic scatter by a forward directed flux and an isotropically scattered flux is shown to give adequate estimates of transfer, and several criteria for estimating the fraction of isotropic scatter are examined.

NOMENCLATURE

a	particle size parameter
A_i	area of ith surface zone [m^2]
A_p	specific projected area for particle cloud [m^2 kg^{-1}]
B_λ	Planck function for spectral distribution of black body emission [W m^{-3}]
B	dust burden [kg m^{-3}]
$C(\mu)$	cumulative phase function, equation (11)
C_1, C_2	constants for particle size distribution [—, μm]
D	diameter of the cylindrical geometry [m]
E	black emissive power [W m^{-2}]
e_1, e_2	error in hemispherical properties, and difference in hemispherical properties defined by equations (19) and (20), respectively
f	fraction of energy scattered in the forward hemisphere
$f(s)$	mass frequency distribution for particle size
$F(s)$	mass cumulative distribution for particle size
K_a, K_s, K_e	absorption, scattering and extinction coefficient [m^{-1}]
l	probable mean free path [m]
L	length of cylindrical geometry [m]
L_p	thickness of plane parallel geometry [m]
m	complex refractive index, $m = n - in^1$
n	refractive index
n^1	absorption index
N	total number of zones
$p(\theta, \phi), p(\mu)$	phase function
Pe	peakedness defined by equation (35)
$Q_{\to i}$	net radiative transfer to ith zone [W]
$Q_{i=j}$	net radiative interchange from ith zone to jth zone [kW]
Q_c	net radiative transfer to the cylindrical surface [kW]
Q_a, Q_s, Q_e	absorption, scattering and extinction efficiencies
R	random numbers uniformly distributed between 0 and 1
s	particle diameter [μm]
$\overline{S_iS_j}$	direct exchange area between ith and jth zone [m^2]
$\overline{S_iS_j}, \overline{S_iG_j}$	total exchange area between ith and jth zone [m^2]
T	temperature [K]
V_i	volume of ith gas zone [m^3]
W_{ij}	weight assigned for exchange area $\overline{S_iS_j}$ in equation (27)
$\overline{X_iY_j}$	total exchange area between ith and jth zone [m^2]

Greek symbols

α	absorptivity in equation (19) and (20), otherwise fraction of anisotropically scattered energy assumed to scatter isotropically, equation (31)
δ	absolute relative deviation in $\Sigma S_iS_j + \Sigma S_iG_k$, defined by equation (25)
$\bar{\Delta}$	mean difference
Δ_{max}	maximum difference
$\overline{\lvert\Delta Q\rvert}$	modulus of the mean difference in heat transfer estimates
ΔQ_{max}	maximum difference in heat transfer estimates
ε	hemispherical emissivity
θ, ϕ	polar and azimuthal angles
λ	wavelength [μm]
μ	cos θ
ρ	hemispherical reflectivity
ρ_p	density of the particle [kg m^{-3}]
σ	Stefan–Boltzmann constant [W m^{-2} K^{-4}]
τ	hemispherical transmissivity/optical thickness
ω	albedo of scatter

Superscript

*	best estimate in equation (27)
–	average

Subscript

i, j, k	zone number
a	absorption
e	extinction
r	reflected

s	scattered
t	transmitted
T	total
0	exact
L	estimates by Lowe [2]
max	maximum

1. INTRODUCTION

A RECENT review [1] has concluded that the fine fly ash carried in the combustion gases of furnaces fired with pulverized coal (p.c.) can be an important—perhaps dominating—emitter.

The radiative behaviour of a particle is determined by the ratio of its circumference to the wavelength of thermal radiation, called the particle size parameter, $a = \pi s/\lambda$, and the complex refractive index, $m = n - in^1$.

For $a \ll 1.0$, absorption and emission are proportional to the volume occupied by the particles, and scatter can be neglected, e.g. soot in furnaces.

For $a \gg 1.0$, absorption and emission are proportional to the projected area of the particle, and although significant radiation is scattered, its deviation is only very slight and can generally be neglected. Particle properties approach those of a macroscopic surface, e.g. unburnt char in furnaces.

For $a \simeq 1.0$, both absorption and scattering are important. Scatter is predominantly forward with significant sideways and backwards. For most p.c. ashes, 90% of the mass lies between 2 and 100 μm, and at the temperatures found in furnaces, from 1200 to 2000 K, 90% of the thermal radiation spectrum lies between a lower wavelength from 1.6 to 0.9 μm, to an upper wavelength from 10.3 to 5.9 μm. Therefore, taking extreme values

$$0.6 \leqslant a \leqslant 350.$$

Scatter can therefore be significant, particularly the scatter of the long wavelength radiation by the finest ash particles.

The effect of such a fly ash cloud can be predicted from a knowledge of the size distribution of the cloud, the ash concentration, and the radiative properties defined in terms of the complex refractive index of the particles. The complex refractive index contains the (real) refractive index, n, for which experimental data exist for many ash-like materials [2, 3], and the absorption index, n^1, for which there is comparatively little data. A simple estimate suggests that the uncertainty in the absorption index alone can lead to errors of 20% in predicted radiative heat transfer [1].

The literature details many previous studies of relevance.

Several exact and approximate techniques are available for analysing isotropic and anisotropic scatter in media between semi-infinite parallel plates [4–6]. The anisotropic radiative transfer from a particulate cloud in a parallel plane geometry has been studied by Love and Grosh [7], Hsia and Love [8] and Shahrokhi and Wolf [9]. Steward and Guruz [10] applied the Monte Carlo method to the same problem and compared the results with those of Love and Grosh. Later, Lowe [2] used the multiflux technique of Shahrokhi and Wolf to calculate the hemispherical radiative properties of a plane parallel particulate cloud with a particle size distribution and refractive index estimated for fly ash.

There appear to be only two studies considering anisotropic scatter in geometries closer to those of industrial furnaces. Stockham and Love [11] investigated thermal radiative transfer from a cylindrical cloud of absorbing, emitting and anisotropically scattering particles, using the Monte Carlo method. Steward and Guruz [12] also used the Monte Carlo method to analyse the effect of alumina/magnesia/soot particles on radiative transfer in cylindrical furnaces.

The present contribution uses the Monte Carlo method and zoning technique to examine anisotropic scatter in enclosures.

Initially, the cloud and ash properties required for the calculation of radiative transfer are outlined (Section 2), and then the accuracy of the Monte Carlo technique is examined in the plane parallel geometry for which analytical solutions are available (Section 3). Section 4 then presents predictions for cylindrical furnace enclosures, leading to the examination of possible approximations for anisotropic scatter.

2. RADIATIVE PROPERTIES OF A PARTICLE CLOUD

2.1. *Efficiency factors and phase function for a single particle*

For a single particle of diameter s, an absorption efficiency $Q_{a,\lambda,s}$ at wavelength λ, can be defined as the ratio of the energy absorbed by the particle to the energy intercepted by the particle. Similarly, the scattering efficiency, $Q_{s,\lambda,s}$ is the ratio of the energy scattered to the energy intercepted by the particle. The phase function, $p_{\lambda,s}(\theta, \phi)$, is the ratio of energy scattered per unit solid angle in the (θ, ϕ) direction to the total energy scattered and is defined such that

$$1 = \frac{1}{4\pi} \int_0^{\pi} \int_0^{2\pi} p_{\lambda,s}(\theta, \phi) \sin \theta \, d\theta \, d\phi. \qquad (1)$$

For convenience the phase function may be taken to be independent of azimuthal angle ϕ (which is true for spherical particles) and expressed as $p_{\lambda,s}(\mu)$, where $\mu = \cos \theta$. Equation (1) is transformed to

$$\int_{-1}^{1} p_{\lambda,s}(\mu) \, d\mu = 2. \qquad (2)$$

2.2. *Absorption and scattering coefficients for a cloud*

The spectral absorption coefficient, $K_{a,\lambda}$ for a particle cloud is defined as the fraction of radiation absorbed from a beam per unit length. The spectral scattering coefficient, $K_{s,\lambda}$ is defined in a similar manner and the extinction coefficient, $K_{e,\lambda}$ is defined as the sum of the two coefficients $K_{a,\lambda}$ and $K_{s,\lambda}$.

For a particle cloud with a fly ash loading B, the

absorption coefficient is given by

$$K_{a,\lambda} = Q_{a,\lambda} B A_p \tag{3}$$

where $Q_{a,\lambda}$ is the cloud absorption efficiency, and A_p the projected surface area of the cloud, defined as

$$Q_{a,\lambda} = \frac{\int_0^\infty [f(s)/s] Q_{a,\lambda,s}(s)\, ds}{\int_0^\infty [f(s)/s]\, ds}, \tag{4}$$

$$A_p = \frac{1.5 \times 10^6}{\rho_p} \int_0^\infty \frac{f(s)}{s}\, ds, \tag{5}$$

where $f(s)$ is the mass frequency function for the particle size distribution.

The spectral cloud scattering and extinction efficiencies are evaluated similarly, the phase function being integrated over the particle size distribution as follows

$$p_\lambda(\mu) = \frac{\int_0^\infty p_{\lambda,s}(\mu) Q_{s,\lambda,s} [f(s)/s]\, ds}{Q_{s,\lambda} \int_0^\infty [f(s)/s]\, ds}. \tag{6}$$

The single particle absorption, scatter and extinction efficiencies and phase function may be calculated from the Mie thoery [13–15]. These efficiencies are complicated functions of the particle size parameter—and therefore of the wavelength of radiation—and the complex refractive index of the particles. A recent examination [1] of published data of materials chemically similar to fly ash suggests that the real refractive index n is approximately 1.5, but the complex absorption index n^1 may vary from 0.005 to 0.5.

Individual fly ash particles are not homogeneous in shape, size or chemical composition [16], but in order to extend the theoretical treatment to fly ash, we assume that all particles are spherical and of the same chemical composition—a requirement for any experimental estimate of the complex refractive index for a particle cloud in the laboratory or field. Willis [17] has defined the complex refractive index of a particle as the complex refractive index of the material in the form of a sphere having the same scattering pattern as the particle. The definition can be extended to a particle cloud. This definition enables the Mie theory to be applied to a fly ash cloud.

Estimates of cloud efficiencies for typical coarse and fine size distributions of fly ash are presented in Fig. 1. Three distributions, with mass cumulative size distribution, $F(s)$, given by equation (7), have been considered, the mass frequency size distribution function, $f(s)$, being expressed by equation (8)

$$F(s) = C_1 \exp(-C_2/s), \tag{7}$$

$$f(s) = dF(s)/ds = (C_1 C_2/s^2) \exp(-C_2/s). \tag{8}$$

The constants C_1, C_2 for the three distributions are presented in the Appendix with a discussion of the size distribution function. The mass median diameters (50% of the mass being below the mass median diameter), for the distributions are 24, 20 and 11 μm, respectively.

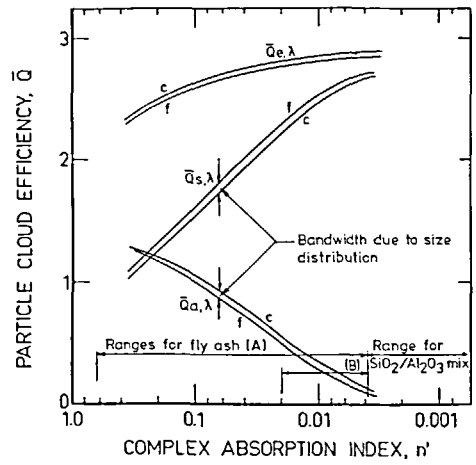

FIG. 1. Variation of the cloud efficiencies at a wavelength of 2.67 μm with the complex absorption index for fine (f) and coarse (c) particle size distributions with ranges indicated for clay mixtures (SiO_2/Al_2O_3), (A) the fly ash range originally proposed by Wall *et al.* [1] and (B) modified by Gupta and Wall [3]. The real refractive index, n has been taken as 1.5.

Figure 1 suggests a primary dependence of the radiative properties on the complex absorption index with a secondary influence of particle size distribution. This conclusion is in agreement with Buckius and Hwang [18] who have demonstrated that cloud efficiencies are relatively independent of particle size distribution for a much wider size range.

2.3. *The effect of temperature on cloud properties*

The total radiative properties of the particle cloud at a particular temperature can be obtained from the (Planck) weighted average of the spectral property. For example, the total cloud absorption efficiency is given by

$$Q_a = \frac{\int_0^\infty Q_{a,\lambda} B_\lambda(T)\, d\lambda}{\int_0^\infty B_\lambda(T)\, d\lambda}, \tag{9}$$

where B_λ is the Planck function for the spectral distribution of black body radiation.

The total scattering and extinction efficiencies for a cloud are evaluated in a similar manner. The phase function for the cloud is also obtained by integration over wavelength, as follows

$$p(\mu) = \frac{\int_0^\infty p_\lambda(\mu) Q_{s,\lambda} B_\lambda\, d\lambda}{Q_s \int_0^\infty B_\lambda\, d\lambda}. \tag{10}$$

Leguerre quadrature has been used for the numerical integration over particle sizes and wavelengths. A fortieth-order quadrature has been found to be sufficient for evaluating spectral properties of the cloud, while a fifth-order quadrature has been used to integrate the spectral properties and efficiencies.

Spectral cloud efficiencies have been calculated at

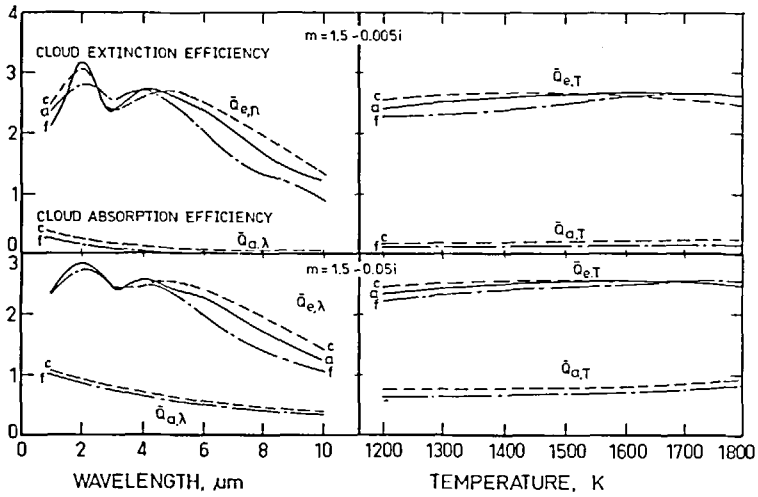

FIG. 2. Variation of the cloud extinction and absorption efficiencies with wavelength and temperature, for coarse (c), average (a) and fine (f) particle size distributions, from equation (8).

wavelengths from 1 to 10μm, and total cloud efficiencies from 1200 to 1800 K for the three particle size distributions and refractive indices of 1.5−0.005i and 1.5−0.05i (see Fig. 2). Figure 2 indicates that the spectral cloud efficiencies vary significantly with wavelength but when integrated over the spectrum according to equation (9) they are fairly constant over the temperature range of interest for furnaces. To allow the cloud efficiency to vary with temperature complicates calculations a great deal, and Fig. 2 indicates that efficiencies at an average furnace temperature might be used rather than allowing them to vary with temperature over the furnace volume. This simplification is used in future sections.

Figure 3 shows the phase function, $p(\mu)$, and cumulative phase function, $C(\mu)$, for the coarse particle size distribution where

$$C(\mu) = \int_{-1}^{\mu} p(\mu)\, d\mu. \tag{11}$$

Figure 3 shows that a higher absorption index results in a more forward directed scatter and as the absorption index decreases, the phase function tends to become circular and the cumulative phase function approaches the linear relation characteristic of isotropic scatter.

3. PLANE PARALLEL GEOMETRY

For media contained between two infinite parallel plates, the hemispherical absorptivity, reflectivity and transmissivity have been calculated numerically for isotropic scatter [6] and anisotropic scatter [2] due to

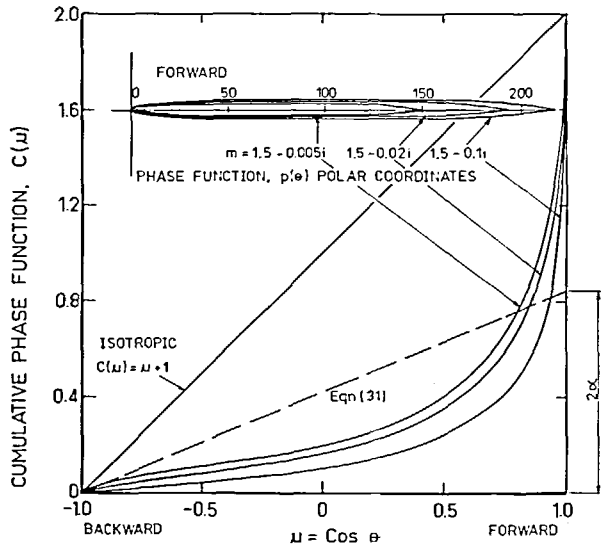

FIG. 3. Phase functions and cumulative phase functions for different complex reflective indices and coarse size distribution of fly ash particle cloud at 1500 K.

fly ash, and these results allow an evaluation of the accuracy and reproducibility of the present Monte Carlo technique.

3.1. *The Monte Carlo method*

The Monte Carlo method is a statistical procedure which can simulate the emission, absorption and scatter of bundles of radiant energy (or photons) as they traverse a gaseous medium. The radiative events are characterized in terms of random numbers $R(0, 1)$ (R in the equations below). Howell [19] has reviewed and discussed, in detail, the application of the Monte Carlo method to radiative transfer. Love and Grosh [7], Steward and Guruz [10], and Plass and Kattawar [20] have applied the Monte Carlo method to anisotropic scattering media.

For computation of the radiative hemispherical properties of a slab by the Monte Carlo method, a fixed number of energy bundles is taken to be emitted from one surface of the slab.

The emission direction of an energy bundle, determined by the azimuthal angle ϕ and polar angle θ, is given by

$$\phi = 2\pi R_1, \tag{12}$$

$$\cos\theta = \sqrt{R_2}, \quad \text{(for a plane surface)}, \tag{13}$$

$$\cos\theta = 1.0 - 2R_3, \quad \text{(for a gas)}. \tag{14}$$

The probable mean free path is given by

$$l = -(1/K_e)\ln R_4, \tag{15}$$

where

$$K_e = K_a + K_s. \tag{16}$$

If, after travelling the distance given by the probable mean free path, the energy bundle has intercepted the opposite side of the slab, then it is assigned to the tally of bundles transmitted. Although not considered in the present study, the reflections off bounding surfaces can be taken into account by comparing the reflectivity with another random number and re-emitting the bundle from the surface if it is not absorbed. If the bundle is not transmitted, another random number, R_5, is compared with the albedo of scatter

$$\omega = K_s/K_e, \tag{17}$$

and if R_5 is less than ω, then the bundle is assigned to the tally of those absorbed, otherwise the bundle is scattered. For isotropic scatter, this event is treated as a new emission, using equations (12) and (14). For anisotropic scatter, the cumulative phase function from

$$C(\mu) = 2.0R_6, \tag{18}$$

determines the new direction of the bundle with respect to the incident direction. Equation (15) assigns the bundle a new mean free path. The bundle is then followed until it reaches a boundary (transmission or reflection) or is absorbed. An energy bundle reaching the surface of emission after single or multiple scatter is considered as reflected by the slab. The proportion of bundles assigned to the three possible fates determines the transmissivity, absorptivity and reflectivity of the slab.

Table 1. Effect of number of bundles emitted on the accuracy of the Monte Carlo method for isotropic scatter in the plane parallel geometry

No. of bundles	$\bar{e}_1$	$e_{1,\max}$
500	0.0346	0.1012
1000	0.0337	0.0812
2500	0.0189	0.0576
5000	0.0123	0.0456
7500	0.0109	0.0432
10000	0.0110	0.0272

3.2. *Isotropic scatter*

The accuracy of the above technique was evaluated by comparison of the Monte Carlo predictions with the exact results tabulated by Özişik [6]. The following error criterion has been used

$$e_1 = |\alpha - \alpha_0| + |\rho - \rho_0| + |\tau - \tau_0|, \tag{19}$$

with the average, $\bar{e}_1$, and maximum, $e_{1,\max}$, for 50 cases ($\omega = 0.1, 0.2, 0.3, 0.4, 0.5, 0.6, 0.7, 0.8, 0.9, 0.95$; $K_eL_p = 0.1, 0.5, 1.0, 2.0, 5.0$) being given in Table 1. Figure 4 shows the comparison for the case with 2500 energy bundles. No trend is observed regarding the behaviour of the error with respect to the albedo of scatter and the extinction coefficient. As expected, the error decreases with an increase in the number of energy bundles considered.

3.3. *Anisotropic scatter*

Lowe [2] has previously calculated the hemispherical properties of plane parallel particle clouds with the coarse particle size distribution, for optical thicknesses of 0.5, 1.0, 2.0, 4.0 and 8.0 and complex refractive indices of 1.437−0.307i, 1.50−0.05i, 1.50

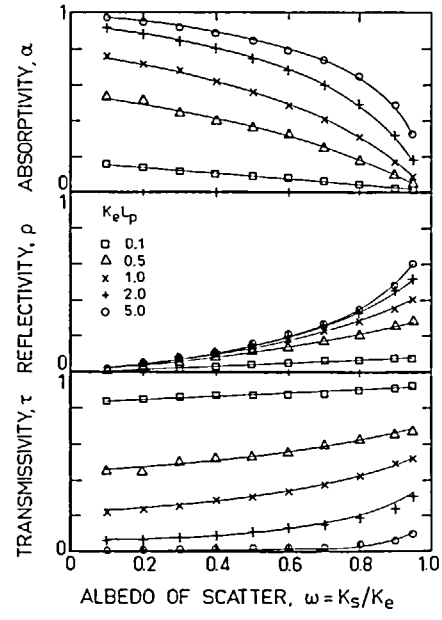

FIG. 4. Comparison of the hemispherical properties of a slab by the Monte Carlo method tracking 2500 energy bundles (points) and Özişik's data [6] (lines) for isotropically scattering media.

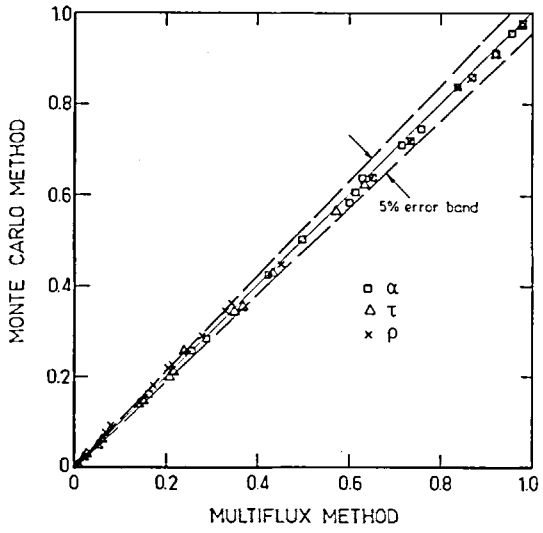

FIG. 5. Comparison of the hemispherical properties of a slab by the Monte Carlo method and multiflux method of Lowe for anisotropic scattering media.

$-0.01i$ and $1.50-0.005i$, at wavelengths 1.3537, 2.6671 and 6.7865 μm. Lowe used the multiflux method similar to that used by Shahrokhi and Wolf [9] with 16 discrete directions to convert the radiative transfer equation into a set of ordinary differential equations, which were solved by standard finite difference schemes. Lowe's solution technique gave hemispherical properties of isotropically scattering slabs in excellent agreement with the exact solutions, and the heat transfer results for anisotropically scattering media were in good agreement with those of Hsia and Love [8]. Therefore, Lowe's results have been used here to evaluate the Monte Carlo method for anisotropic scatter. The Monte Carlo method has been applied to all the cases mentioned above. For the spectral hemispherical properties, $\bar{e}_2$ and $e_{2,\max}$, for the 60 cases were 0.0209 and 0.0785, respectively for 2500 bundles.

$$e_2 = |\alpha-\alpha_L|+|\rho-\rho_L|+|\tau-\tau_L|. \quad (20)$$

The total hemispherical properties were obtained by integrating the spectral hemispherical properties over wavelength in a manner similar to equation (9). Figure 5 shows that the present Monte Carlo results fall within 5% of Lowe's results.

The total hemispherical properties may also be obtained by using the total efficiencies and the total phase functions, from equations (9) and (10), in the Monte Carlo simulation. The total hemispherical properties thus obtained may be compared with those from integration of the spectral hemispherical properties of the cloud over all wavelengths, for complex refractive indices $m = 1.437-0.307i$ and $1.5-ki$, where $k = 0.1$, 0.05, 0.02, 0.01 and 0.005, and cloud thicknesses of 0.5, 1.0, 1.5, 2.0, 4.0, 6.0, 8.0 and 12.0. This comparison gives an average difference, defined in a similar way to equations (19) and (20), of 0.0214 with a standard deviation of 0.016 for the 48 cases. This suggests that the use of total cloud efficiencies and total phase functions for radiative transfer problems is quite adequate for the range of parameters investigated here.

4. CYLINDRICAL GEOMETRY

4.1. *Isotropic scatter in cylindrical geometry*

A common technique for the solution of radiative transfer in enclosures is the zone method, detailed by Hottel and Sarofim [13]. The enclosure is divided into gas and surface zones of constant radiative properties and temperatures. The direct radiative transfer between zones in a non-reflecting enclosure and non-scattering medium is proportional to the difference in the emissive powers of the two zones:

$$Q_{i\rightleftharpoons j} = \overline{s_i s_j}(E_i - E_j). \quad (21)$$

The proportionality constant $\overline{s_i s_j}$ is termed the direct exchange area. The net radiative transfer between any two zones in a scattering medium bounded by reflecting surfaces must take into account the emissivity of the enclosure walls and the scattering properties of the medium. A total interchange area can therefore be defined which accounts for these properties:

$$Q_{i\rightleftharpoons j} = \overline{S_i S_j}(E_i - E_j). \quad (22)$$

Hottel and Sarofim [13] have detailed a method by which $\overline{S_i S_j}$ may be calculated from $\overline{s_i s_j}$ in an enclosure with reflecting surfaces and an isotropically scattering medium. Data for direct exchange areas is available for simple zone shapes, e.g. square, cube, cylindrical and annular [13] and therefore the method is restricted to enclosures of these shapes. Although the method is probably the most common for non-scattering media, it has rarely been used for scattering media.

The Monte Carlo technique has been previously used by Gupta and Datta [21] for the computation of direct and total exchange areas in cylindrical geometries for gray gases. By this method the total exchange area $\overline{S_i S_j}$ is estimated as the ratio of the net number of energy bundles received by zone j to the total number of bundles emitted by zone i. Being a statistical method, the exchange areas obtained by this technique will necessarily be in error and the following conservation relationship will not hold exactly:

$$\overline{S_i S_j} = \overline{S_j S_i}, \quad (23)$$

$$\sum_j \overline{S_i S_j} + \sum_k S_i G_k = A_i \varepsilon_i,$$

$$\sum_j \overline{G_i S_j} + \sum_k \overline{G_i G_k} = 4K_e(1-\omega)V_i. \quad (24)$$

The exchange areas should therefore be normalized before proceeding to calculate the radiative heat transfer.

Vercommen and Froment [22] have described a least-square technique to normalize the exchange areas. This method requires the solution of $N \times (N-1)/2$ simultaneous linear algebraic equations (that is, the inversion of an $N \times (N-1)/2$ order matrix where N is the number of zones).

A simpler alternative offered here is as follows:

(1) First of all, the symmetric relationship, described by equation (23), is enforced by substituting $\overline{S_iS_j}$ and $\overline{S_jS_i}$ by their averaged value.

(2) For each surface zone calculate

$$\delta_i = \left| \frac{\sum \overline{S_iS_j} + \sum \overline{S_iG_k} - A_i\varepsilon_i}{A_i\varepsilon_i} \right|. \quad (25)$$

(3) Normalize the exchange area row and column of highest δ_i in the following manner

$$\overline{S_iS_j}\Big|_{\text{normalized}} = \frac{\overline{S_iS_j}A_i\varepsilon_i}{\sum \overline{S_iS_j} + \sum S_iG_k}. \quad (26)$$

Repeat this normalization scheme with rows and columns for decreasing δ_i. This technique has been compared to that of Vercommen and Froment's [22], the difference in exchange areas by the two methods being defined by the following relation which sums the weighted difference between all (N) surface/surface, gas/surface and gas/gas total exchange area combinations:

$$\Delta = \frac{1}{N}\sum_N \left(\left| \frac{\overline{X_iY_j} - \overline{X_iY_j}^*}{\overline{X_iY_j}} \right| \times W_{ij} \right), \quad (27)$$

where

$$\overline{X_iY_j} = \overline{S_iS_j}, \overline{S_jS_i}, \overline{G_iS_j}, \overline{G_jS_i}, \overline{G_iG_j}, \overline{G_jG_i}, \quad (28a)$$

and

$$W_{ij} = \frac{\overline{X_iY_j}^*}{A_i\varepsilon_i} \quad \text{for } i \text{ a surface zone,} \quad (28b)$$

and

$$W_{ij} = \frac{\overline{X_iY_j}^*}{4K_{a,i}V_i} \quad \text{for } i \text{ a gas zone.} \quad (28c)$$

$\overline{X_iY_j}^*$ is the best estimate for the exchange area, being that by the Hottel and Sarofim [13] method for isotropic scatter. Although it will later be shown that the Hottel and Sarofim method may also be in error, a valid comparison of the normalization techniques can be made with this common basis.

The weighting W_{ij} is used to suppress any undue increase in Δ due to very small exchange areas, in which relative error is comparatively very high, though these exchange areas are of little significance in overall heat transfer.

The total exchange areas for a cylindrical furnace with an L/D of 0.5 [as shown on Fig. 6(b)] were estimated by the two normalization techniques for extinction coefficients of 0.1, 0.25, 0.5, and 0.75 m^{-1} and albedos of scatter of 0.2, 0.5, 0.8 and 0.9. The enclosure walls were assigned an emissivity of unity so as to study the effect of scatter of the cloud alone.

Table 2 summarizes the statistics for the 16 cases, indicating that the two normalizations are of comparable accuracy. The computation time for normalization is approximately proportional to the sixth power of the number of zones in Froment's technique, while in this present technique it is directly proportional. We suggest that computational economy justifies the use of our alternative simple procedure.

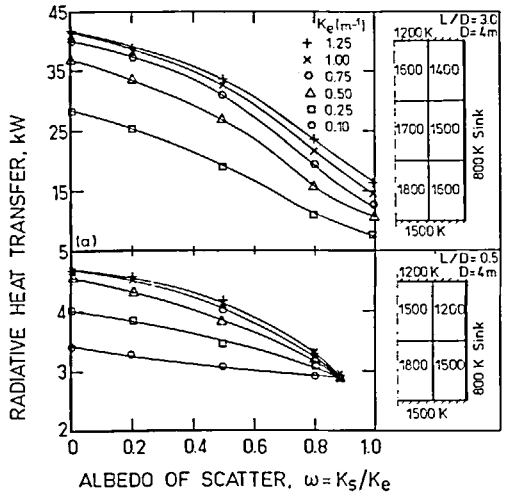

FIG. 6. Isotropic scatter—the predicted radiative heat transfer to a sink at 800 K in two cylindrical furnaces zoned as indicated.

Figure 7 presents the difference in the total exchange areas, computed by the zone method and the Monte Carlo technique using the normalization of equation (26) for a cylindrical geometry with $L/D = 3.0$. Twelve axial subdivisions were used in the zone method. Figure 7 demonstrates that the difference in the total exchange areas increases with the albedo of scatter, and this increase becomes much more pronounced at high extinction coefficients. This suggests that at high extinction coefficients and higher albedos of scatter, the zone method requires even a finer zoning subdivision than used here, and that the Monte Carlo technique might be preferred in scattering systems.

To conclude the calculation, after having obtained the total exchange areas, the radiative transfer to any zone can be computed from the following equations

$$Q_{\to i} = -A_i\varepsilon_iE_i + \sum_j \overline{S_iS_j}E_j + \sum_k \overline{S_iG_k}E_k \quad (29)$$

if i is a surface zone,

$$Q_{\to i} = -4K_e(1-\omega)V_iE_i + \sum_j \overline{G_iS_j}E_j + \sum_k \overline{G_iG_k}E_k \quad (30)$$

if i is a volume zone.

These equations have been used to predict the net radiative transfer to the cylindrical surface for cylindrical geometries with L/D ratios of 0.5 and 3.0 and the zoning and temperature profiles shown in Fig. 6. The influence of the extinction coefficient K_e and the

Table 2. Comparison of the estimates of total exchange areas $\overline{S_iS_j}$ by the least squares technique of ref. [22] and the present technique [equations (25) and (26)]

Statistic	Least squares technique	Present technique
Average, $\bar{\Delta}$	0.0111	0.0134
Standard deviation of Δ	0.0054	0.0057
Maximum	0.0268	0.0262

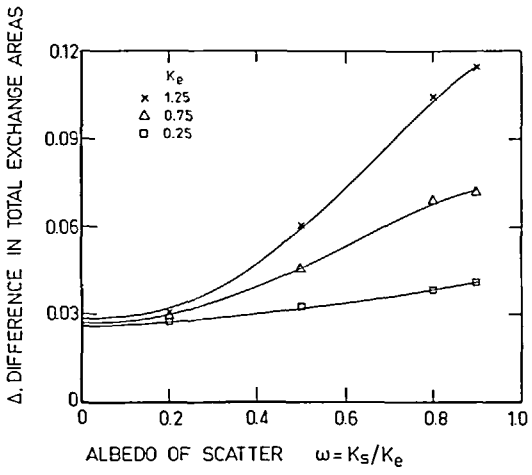

FIG. 7. Difference in the total exchange areas by the Monte Carlo and by the Hottel and Sarofim technique for isotropic scattering in cylindrical geometry (L/D = 3.0 of Fig. 6), from equation (27).

scattering albedo demonstrates that the net radiative transfer to the sink zone (i.e. cylindrical surface) decreases as the albedo of scatter increases and the rate of increase of transfer with albedo of scatter is a function not only of the extinction coefficient but also of L/D.

4.2. *Anisotropic scatter in cylindrical geometry*

The conclusions of the previous sections suggest the following procedure for the estimation of radiative heat transfer by fly ash in furnaces by the Monte Carlo method:

(1) Use Mie theory to calculate the cloud efficiencies and the cloud phase function for a mean gas temperature and measured particle size distribution, and the effective complex absorption index of the particles. An effective complex refractive index can account for the heterogeneity of fly ash as discussed in Section 2.2.

(2) Divide the enclosure into a number of zones and compute the total exchange areas, normalized according to equation (26).

(3) Iterate through the heat balances for the temperature of each zone by the usual technique described by Hottel and Sarofim [13] and calculate the net radiative transfer to the heat sinks (absorbing walls) of the furnace using equations (29) and (30). If the temperature distribution is known the iterative step is omitted.

A more accurate alternative could be to use the spectral cloud efficiencies instead of the efficiencies at a mean gas temperature and to obtain the radiative transfer by integrating the spectral radiative exchange between each zone. Fortunately, a comparison of the hemispherical radiative properties for plane parallel slabs, calculated by these two methods detailed in Section 3.3 suggests that such an elaborate procedure is not warranted.

The predictions using the procedure 1–3 above for the radiative transfer to the sink of the furnace sketched

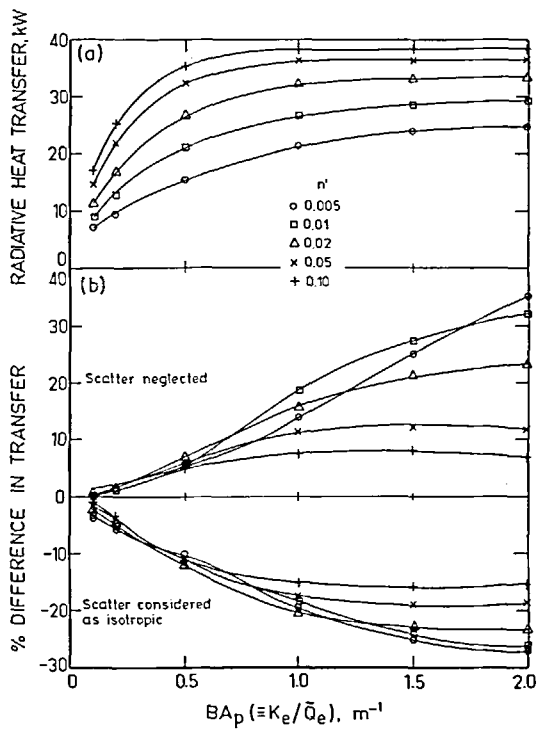

FIG. 8. Predicted radiative transfer to the sink of the furnace of Fig. 6 with L/D = 3. Coarse ash size distribution, with cloud properties estimated at 1500 K.

on Fig. 6 with an L/D = 3, and diameter of 4 m—corresponding to the shape of an end fired industrial furnace—are shown on Fig. 8(a). Figure 8(b) compares these estimates with those made using two extreme simplifying assumptions regarding scatter: the scatter is neglected completely ($K_e = K_a$); the scatter is isotropic with $p(\mu) = 1$; and $C(\mu) = \mu + 1$, as shown on Fig. 2.

Neglecting scatter is seen to overestimate transfer, while considering scatter to be isotropic underestimates transfer. Both estimates depend on the absorption index, n^1, and the multiple of the dust burden with the cloud projected area, BA_p; neither gives adequate predictions for engineering calculations. The projected area A_p for fly ash may range from 75 to 125 $m^2\,kg^{-1}$ while the dust burden may vary from 2 to 20 g m^{-3}. The range of interest on Fig. 8 is therefore $0.15 < BA_p\,[m^{-1}] < 2.5$.

5. SIMPLE MODELS FOR ANISOTROPIC SCATTERING

While the above procedures with the two extreme simplifying assumptions do not give adequate predictions—both resulting in errors of up to 30% over the range of parameters of practical interest—the results of Fig. 8 suggest that a weighting might be assigned to the results for each extreme. In fact, the average of the 'scatter neglected' and 'isotropic scatter' extremes appears, from Fig. 8, to be such a possibility. The ease with which radiative heat transfer can be

calculated for the extremes, compared to the difficulty of handling anisotropic scatter, certainly justifies the investigation of this possibility.

There have been several attempts to reduce the highly anisotropic phase function to simple phase functions, i.e. a delta function in the forward direction together with a much simpler phase function [23]. The simpler phase function, in general, has been taken as a linear anisotropic phase function [24, 25], commonly known as the δ-Eddington approximation. Lee and Buckius [26] have also described scaling factors for converting an anisotropic scatter problem to an isotropic scatter problem. In the present work similar approximations will be investigated.

Anisotropically scattered radiation can be approximated by a sum of isotropically scattered and forward directed components. If α is the fraction of anisotropically scattered radiation assumed to scatter isotropically and the balance is forward directed, then the phase function can be written as

$$p(\mu) = \alpha + 2(1-\alpha)\delta(\mu-1), \tag{31}$$

where $\delta(\mu-1)$ is a Dirac delta function that satisfies the following equation

$$\int_{-\infty}^{\infty} f(x)\delta(x-x_1)\,dx = f(x_1). \tag{32}$$

Anisotropic scattering with a scattering coefficient K_s and phase function given by equation (31) is exactly equivalent to isotropic scattering with a scattering coefficient αK_s. The application of the following simple models therefore involves the calculation for isotropic scatter only, but with αK_s being used as the scattering coefficient.

A number of criteria for estimating α which are based on the gross characteristics of the simplified phase function given by equation (31) and the actual phase function can now be examined.

(1) α may be estimated by equating the fraction of scatter in the forward hemisphere (f) for the simplified and actual phase functions:

$$f = \frac{1}{2}\int_0^1 p(\mu)\,d\mu = 1-\frac{\alpha_1}{2} \tag{33}$$

or

$$\alpha_1 = 2(1-f). \tag{34}$$

This approximation is equivalent to the two flux approximation of Lee and Buckius [26].

(2) The second alternative equates the peakedness, (Pe), defined as the ratio of the second and zeroth moment of the phase function in the forward direction (ref. [13], p. 434). That is

$$Pe = \frac{1}{2}\frac{\int_0^1 \mu^2 p(\mu)\,d\mu}{f}, \tag{35}$$

and

$$\alpha_2 = (1-Pe)\Big/\left(\frac{5}{6}-\frac{Pe}{2}\right). \tag{36}$$

(3) Another alternative is provided by analogy with the well-known six-flux method for approximating radiative transfer. This considers scatter in six mutually perpendicular directions—forward, backward and to the four sides (ref. [13], p. 433). The difference between the fraction scattered in the forward and backward directions may then be approximated as $(1-\alpha)$ to give

$$1-\alpha_3 = \frac{\int_0^1 \mu^2 p(\mu)\,d\mu - \int_{-1}^0 \mu^2 p(\mu)\,d\mu}{\int_{-1}^1 p(\mu)\,d\mu}, \tag{37}$$

or

$$\alpha_3 = 1-\frac{1}{2}\left[\int_0^1 \mu^2 p(\mu)\,d\mu - \int_{-1}^0 \mu^2 p(\mu)\,d\mu\right]. \tag{38}$$

(4) Equating the area under cumulative phase functions gives

$$\int_{-1}^1 C(\mu)\,d\mu = 2-\int_{-1}^1 \mu p(\mu)\,d\mu = 2\alpha_4, \tag{39}$$

so that

$$\alpha_4 = 1-\frac{1}{2}\int_{-1}^1 \mu p(\mu)\,d\mu = 1-\langle\mu\rangle, \tag{40}$$

where $\langle\mu\rangle$ is equal to half the first moment of the phase function and is termed as the asymmetry factor.

This approximation has been considered by Lee and Buckius [26] and has been shown to be the best among their approximations for a plane parallel geometry.

(5) The final alternative uses the least squares criterion to minimize the deviation of the simplified cumulative phase function from the actual cumulative phase function, that is

$$\min\left\{\int_{-1}^1 [C(\mu)-\alpha(1+\mu)]^2\,d\mu\right\}. \tag{41}$$

The value of α that satisfies the above expression is evaluated from

$$\int_{-1}^1 [C(\mu)-\alpha(1+\mu)](1+\mu)\,d\mu = 0. \tag{42}$$

Equation (42) can be simplified to give

$$\alpha_5 = \frac{1}{16}\left[18-6\int_{-1}^1 \mu p(\mu)\,d\mu - 3\int_{-1}^1 \mu^2 p(\mu)\,d\mu\right]. \tag{43}$$

For the given particle size distribution, Table 3 compares the five estimates for α for various complex absorption indices. These simple models are evaluated by comparing predictions obtained using the exact phase function and the approximate phase function

Table 3. Comparison of the estimates for α

n^1	α_1	α_2	α_3	α_4	α_5
0.005	0.165	0.556	0.352	0.280	0.316
0.01	0.153	0.545	0.338	0.267	0.304
0.02	0.136	0.527	0.315	0.245	0.284
0.05	0.103	0.484	0.269	0.204	0.242
0.10	0.079	0.436	0.228	0.168	0.204

Table 4. Difference (%) between estimates of hemispherical properties of a plane parallel geometry for anisotropic scatter and the simple models for anisotropic scatter

n^1	α_1	α_2	α_3	α_4	α_5
0.005	17.13	24.27	7.01	1.71	3.31
0.01	14.12	22.55	7.59	2.18	4.36
0.02	10.69	21.05	7.11	2.14	4.53
0.05	8.02	14.06	2.82	1.75	0.80
0.10	5.28	9.91	2.04	1.42	0.75

given by equation (31) in the plane parallel geometry as well as in the cylindrical geometry.

Table 4 presents the comparison of hemispherical properties for a plane parallel geometry with BA_p varying from 0.5 to 12.0 m^{-1}, using the various estimates for α. The difference in the estimates of the properties does not vary significantly within this range of BA_p, while the difference in the estimates increases with an increase in scattering albedo (i.e. lower absorption index). α_1 was found to underestimate the hemispherical absorptivity and transmissivity, while α_2 overestimates these. The comparison demonstrates the superiority of the approximation by α_4 for this geometry, but α_3 and α_5 also give reasonable estimates.

In the cylindrical geometry [see Figure 6(a)], α_1 overestimates the radiative transfer while α_2 underestimates transfer. The error increases for high values of BA_p and low values of the absorption index.

Table 5 presents the statistics for the comparison of radiative transfer and exchange areas for the five approximations for thin ($BA_p \leqslant 0.5$) and thick ($BA_p \geqslant 1.0$) fly ash clouds. Table 5 suggests that for thin clouds (equivalent to a dust burden of 5 g m^{-3} with a projected area of 100 m^2 kg^{-1}) α_3 is the best approximation. For higher dust burdens, α_5 is the best approximation, but α_3 and α_4 also give reasonable predictions (within 5%) which are quite adequate for engineering calculations of heat transfer.

6. CONCLUSIONS

For the calculation of radiative transfer in furnaces the particle cloud efficiencies for fly ash clouds may be assigned at a mean furnace temperature. The efficiencies are primarily dependent on the complex absorption index with a secondary dependence on the size distribution of the fly ash and the temperature, with the present uncertainties in the absorption index having greater effect than the known variation of size and temperatures.

The Monte Carlo technique can be used for the calculation of radiative heat transfer in scattering media with an accuracy determined by the number of energy bundles tracked. For anisotropic scatter, characteristic of all fine dielectric particles and fly ash in particular, no other technique appears able to handle the complexity necessary for calculations in furnace enclosures. Neglecting scatter overestimates transfer while considering scatter to be isotropic underestimates transfer.

Approximating anisotropic scatter by a forward directed flux and an isotropically scattered flux can give adequate engineering estimates of radiative heat transfer.

Acknowledgements—The authors are thankful to NERDDC for financial support.

REFERENCES

1. T. F. Wall, A. Lowe, L. J. Wibberley, T. Mai-Viet and R. P. Gupta, Fly ash characteristics and radiative heat transfer in pulverised-coal-fired furnaces. *Combust. Sci. Technol.* **26**, 107–121 (1981).
2. A. Lowe, Measurement and analysis of radiative properties of fly ash particles in pulverised coal furnaces and their effect on heat transfer, Ph.D. thesis, University of Newcastle (1978).
3. R. P. Gupta and T. F. Wall, The complex refractive index of particles, *J. Phys. D: Appl. Phys.* **14**, L95–8 (1981).
4. V. N. Adrianov, Differential methods of radiant heat transfer calculations, *Heat Transfer—Sov. Res.* **1**, 111–125 (1969).
5. G. E. Hunt, A review of computational techniques for analysing the transfer of radiation through a model cloudy atmosphere, *J. Quantve Spectros. Radiat. Transfer* **11**, 655–690 (1971).
6. M. N. Özişik, *Radiative Transfer*. Wiley Interscience, New York (1973).
7. T. J. Love and R. J. Grosh, Radiative heat transfer in absorbing, emitting, and scattering media, *J. Heat Transfer* **87C**(5), 161–166 (1965).

Table 5. Statistical comparison of simple models for anisotropic scatter in the cylindrical geometry

Statistic		α_1	α_2	α_3	α_4	α_5
15 cases with $BA_p \leqslant 0.5$						
$\%\Delta Q$	average	1.34	−2.07	0.06	0.43	0.33
	S.D.	1.59	1.33	0.58	1.03	0.98
	max	4.75	−4.28	1.07	2.36	2.05
$\%\Delta EA$	average	4.86	7.15	4.43	4.27	4.48
	S.D.	1.63	2.31	0.87	1.22	1.01
	max	8.03	12.24	6.26	6.62	6.67
25 cases with $BA_p \geqslant 1.0$						
$\%\Delta Q$	average	9.05	−8.66	0.93	2.42	0.53
	S.D.	4.06	2.79	1.09	1.12	0.89
	max	17.57	−14.76	−3.29	5.26	2.81
$\%\Delta EA$	average	8.92	11.95	4.41	3.68	3.68
	S.D.	3.01	2.97	0.96	0.87	0.87
	max	13.57	17.51	6.41	6.02	5.65

8. H. M. Hsia and T. J. Love, Radiative transfer between parallel plates separated by nonisothermal medium with anisotropic scattering, *J. Heat Transfer* **89C**(8), 197–204 (1967).
9. F. Shahrokhi and P. Wolf, Numerical solution to the radiation heat transfer equation for scattering medium, *AIAA J.* 6(9), 1748–1752 (1968).
10. F. R. Steward and K. H. Guruz, Radiative heat transfer in absorbing, emitting and scattering media using the Monte Carlo method, *Trans. Can. Soc. Mech. Engng* 3(1), 10–16 (1975).
11. L. W. Stockham and T. J. Love, Radiative heat transfer from a cylindrical cloud of particles, *AIAA J.* 6(10), 1935–1940 (1968).
12. F. R. Steward and K. H. Guruz, The effect of solid particles on radiative transfer in cylindrical test furnaces, Fifteenth Int. Symp. on Combustion, p. 1271 (1974).
13. H. C. Hottel and A. F. Sarofim, *Radiative Transfer*. McGraw-Hill, New York (1967).
14. H. C. Van de Hulst, *Light Scattering by Small Particles*. Wiley, New York (1957).
15. M. Kerker, *Scattering of Light and Electromagnetic Radiation*. Academic Press, London (1970).
16. P. J. Wyatt, Some chemical, physical and optical properties of fly ash particles, *Appl. Optics* **19**, 975–983 (1980).
17. C. Willis, the complex refractive index of particles in a flame, *J. Phys. D: Appl. Phys.* **3**, 1944–1956 (1970).
18. R. O. Buckius and D. C. Hwang, Radiation properties for polydispersions: application to coal, *J. Heat Transfer* **102**, 99–103 (1980).
19. J. R. Howell, Application of Monte Carlo to heat transfer problems, *Adv. Heat Transfer* **5**, 2–54 (1968).
20. G. N. Plass and G. W. Kattawar, Monte Carlo calculations of light scattering from clouds, *Appl. Optics* 7(3), 415–419 (1968).
21. R. P. Gupta and A. Datta, Application of Monte Carlo method for exchange areas and zoning method for heat flux and temperature distribution in a cylindrical furnace, presented at 30th Annual Conference of Indian Institute of Chem. Engrs in Cochin, India (1978).
22. H. A. J. Vercommen and G. F. Froment, An improved zone method using Monte Carlo techniques for the simulation of radiation in industrial furnaces, *Int. J. Heat Mass Transfer* **23**, 329–337 (1980).
23. B. H. J. McKellar and M. A. Box, The scaling group of radiative transfer equation. *J. Atmos. Sci.* **38**, 1063–1068 (1981).
24. J. H. Joseph, W. J. Wiscombe and J. A. Weinman, The delta-Eddington approximation of radiative flux transfer, *J. Atmos. Sci.* **33**, 2452–2459 (1976).
25. M. F. Modest and F. H. Azad, The influence and treatment of Mie anisotropic scattering in radiative transfer, *J. Heat Transfer* **102C**, 92–98 (1980).
26. H. Lee and R. O. Buckius, Scaling anisotropic scattering in radiation heat transfer for a planar medium, *J. Heat Transfer* **104C**, 68–75 (1982).

APPENDIX

Lowe [2] studied the particle size distribution of fly ashes from a number of power stations in NSW. A bimodal log-normal distribution was found to fit the size distribution for fly ashes accurately, by least square fit. The least square technique was also used to fit the experimental data to an empirical discontinuous function of the form

$$F(s) = C_1 \exp(-C_2/s), \quad 0 < s < s_1, \tag{A1a}$$

$$= \exp(-C_2'/s), \quad s_1 < s < \infty. \tag{A1b}$$

The constants in equations (A1a) and (A1b), and the statistics of the fit are presented in Table A1. Table A2 presents the mass median and RMS diameters for these distributions, and mass fraction and the area fraction expressed by equation (A1a). The particle cloud of RMS diameter 2.75 μm, has about 35% greater projected area as compared to that of RMS diameter 3.68 μm.

The radiative properties of a particle cloud depend on the projected area and equation (A1a) expresses more than 90% of the area for all three distributions. Therefore equation (A1a) may be extended to equation (A2)

$$F(s) = C_1 \exp(-C_2/s), \quad 0 < s < \infty. \tag{A2}$$

This expression represents the size distribution at the fine end and the cumulative area distribution up to about 92% very accurately.

Equation (A2) [which is the same as equation (7) in Section 2.2], is therefore used for evaluating the cloud efficiencies.

Table A1. Constants for empirical equations (A1a) and (A1b) for some ash size distribution for three power station coals. Adapted from Lowe [2]

Station coal	Equation for $F(s)$	Size range (μm)	Standard error (%)
Wallerawang	$0.929 \exp(-6.742/s)$	0–37	3.2
	$1.0 \exp(-9.470/s)$	37+	2.3
Liddell	$0.743 \exp(-7.814/s)$	0–40	1.9
	$1.0 \exp(-19.70/s)$	40+	2.3
Munmorah	$0.726 \exp(-8.750/s)$	0–35	1.6
	$1.0 \exp(-19.96/s)$	35+	2.5

Table A2. Mass median diameters, range of validation for, and mass and area fraction expressed by equation (A1a)

Station coal	Mass median diameter (μm)	RMS diameter (μm)	s_1 (μm)	$F(s_1)$	Area fraction expressed by equation (A1a)
Wallerawang	11	2.76	37	0.77	0.98
Liddell	20	3.25	40	0.61	0.95
Munmorah	24	3.65	35	0.56	0.93

DIFFUSION DU RAYONNEMENT PAR LES POUSSIERES VOLANTES DANS LES FOYERS A CHARBON PULVERISE: APPLICATION DE LA METHODE DE MONTE CARLO A LA DIFFUSION ANISOTROPE

Résumé—Les propriétés d'absorption, de diffusion et d'extinction d'un nuage de poussière volante sont principalement liées à l'indice complexe d'absorption des particules avec une dépendance secondaire à la température et à la distribution des tailles des particules. La méthode de Monte Carlo est utilisée pour calculer le transfert radiatif dans des volumes de plaque et de cylindre. Une diffusion anisotrope approchée par un flux dirigé en avant plus un flux de diffusion isotrope donne des estimations correctes du transfert, et on examine plusieurs critères pour évaleur la fraction de diffusion isotrope.

STRAHLUNGSSTREUUNG DURCH FLUGASCHE IN KOHLENSTAUB-GEFEUERTEN ÖFEN: ANWENDUNG DES MONTE-CARLO-VERFAHRENS AUF ANISOTROPE STREUUNG

Zusammenfassung—Es wird gezeigt, daß die Wirkungsgrade von Absorption, Streuung und Extinktion einer Flugaschenwolke in erster Linie vom komplexen Absorptions-Index der Partikel abhängen und in zweiter Linie von der Verteilung von Temperatur und Partikelgröße. Weiterhin wird dann mit Hilfe des Monte-Carlo-Verfahrens der Strahlungswärmeaustausch in rechteckigen und zylindrischen Brennkammern berechnet. Eine angemessene Abschätzung der Austauschvorgänge läßt sich dadurch erzielen, daß die anisotrope Streuung durch einen direkten und einen isotrop gestreuten Strahlungsfluß angenähert wird. Einige Kriterien zur Abschätzung des Anteils der isotropen Streuung werden untersucht.

РАССЕЯНИЕ ЛУЧИСТОГО ПОТОКА ЛЕТУЧЕЙ ЗОЛОЙ В ПЫЛЕУГОЛЬНЫХ ТОПКАХ: ПРИМЕНЕНИЕ МЕТОДА МОНТЕ КАРЛО ДЛЯ РАСЧЕТА АНИЗОТРОПНОГО РАССЕЯНИЯ

Аннотация—Показано, что поглощение, рассеяние и "гашение" пламени облаком летучей золы в основном зависит от сложного характера показателя поглощения частиц и дополнительно от температуры и распределения частиц по размерам. Методом Монте Карло рассчитывается лучистый перенос в плоской и цилиндрической полостях топок. Показано, что аппроксимация анизотропного рассеяния потоком "вперед" и изотропно рассеянным потоком позволяет получить адекватные оценки переноса. Рассмотрено несколько критериев для определения доли изотропного рассеяния.